7828 *Macromolecules* **2009**, *42*, 7828–7835
DOI: 10.1021/ma9012303

Macromolecules
ARTICLE

Environmentally Compliant Fluoro-Containing MMA/nBA Colloidal Dispersions; Synthesis, Molecular Modeling, and Coalescence

Anuradha Misra and Marek W. Urban*

School of Polymers and High Performance Materials Shelby F. Thames Polymer Science Research Center The University of Southern Mississippi Hattiesburg, Mississippi 39406

Received June 8, 2009; Revised Manuscript Received September 20, 2009

ABSTRACT: While aqueous phase colloidal synthesis of F-containing dispersions is often restricted by low solubility and surface tension of monomers, the use of bioactive dispersing agents, such as phospholipids, may alleviate these problems. Using 1,2-dilauroyl-*sn*-glycero-3-phosphocholine (DLPC), we copolymerized heptafluorobutyl methacrylate (FBMA), heptafluorobutyl acrylate (FBA), heptadecafluorodecyl methacrylate (FMA), heptadecafluorodecyl acrylate (FA) with methyl methacrylate (MMA) and *n*-butyl acrylate (nBA) monomers which resulted in the formation of stable nonspherical colloidal dispersions that contain up to 15% (w/w) of the fluoropolymer (FP) phase. These studies report for the first time an aqueous phase FP colloidal dispersion synthesis without the use of fluoro-dispersing agents. Experimentally determined by transmission electron microscopy (TEM) particle phase-separated morphologies consist of the FP phase that polymerize on the surface of *p*-MMA/nBA core particles. Thermodynamic molecular modeling simulations show that the coexistence of fluorinated and nonfluorinated segments is energetically favorable and the presence of the FP phase decreases the cohesive energy density of macromolecular chains. These theoretical predictions are in agreement with the experimental results. Nonspherical FP containing colloidal particles coalesce to form stable films with ultra low static and kinetic coefficients of friction as well as the low surface energy which result from stratification of the FP phase near the film−air (F−A) interface. As a result, property gradients are achieved, which are manifested by the low static and kinetic coefficients of friction near the F−A interface due to the presence of the FP phase and lower glass transition temperature (T_g) of *p*-MMA/nBA phase near the film−substrate (F−S) interface. The latter facilitates the flow during coalescence.

Introduction

The use and production of fluoro and chloro-containing polymers was identified as one of the causes for diminishing of the ozone layer due to emission of chlorofluorocarbons (CFCs).[1] The primary problems associated with the production and applications of fluoro and chloro polymers are their insolubility in common organic solvents, thus requiring the use of CFCs during their polymerization. Even under these reaction conditions, copolymerization of fluorinated monomers with hydrophilic or lipophilic comonomers may be troublesome without addition of dispersing agents or suitable cosolvents. Attempts to overcome these conditions have led to the successful development of supercritical CO_2 (SCO) process,[2−4] an attractive alternative for a wide variety of chemical and industrial processes that involve pressurized polymerization conditions.[2,3,5−7] While these efforts have led to new environmentally compliant technologies, the use of F-containing nonpolymerizable species during synthesis is still unavoidable. Ideally, one would like to design environmentally benign FPs that can be applied to a substrate from an aqueous phase to form polymeric films or coatings with the properties characteristics of FPs, but free of low molecular weights F-containing dispersing agents. Unfortunately, low solubility and surface tension of F-monomers often restrict traditional synthetic steps and requires the use of F-surfactants.

In response to these challenges colloidal copolymerization of F-monomers with other monomeric species to form stable colloidal particles using classical emulsion[8−10] and miniemulsion processes[11] were developed. Although several attempts have been made to prepare fluorinated colloidal dispersions, elaborate synthetic procedures, the use of complex starting materials such as cyclodextrin[12,13] or other cosolvents,[14] as well as relatively low % solids and consequently lower FP content, represent significant restrictions.[8−11,15,16] One approach that has partially addressed these problems was the utilization of a combination of fluoro-containing dispersing agents during aqueous copolymerization of acrylate families of monomers.[17−20] However, the use of even small amounts of F-surfactants to stabilize colloidal dispersions, which are often mobile after coalescence,[21] still represents significant environmental concerns.

To entirely eliminate the use of F-surfactants as well as any other potential hazardous components during synthesis, processing, and applications, these studies report for the first time the development of colloidal dispersions without F-surfactants using simple free radical semicontinuous process of the following copolymers: *p*-methyl methacrylate/*n*-butyl acrylate/heptafluorobutyl methacrylate (*p*-MMA/nBA/FBMA), *p*-methyl methacrylate/*n*-butyl acrylate/heptafluorobutyl acrylate (*p*-MMA/nBA/FBA), *p*-methyl methacrylate/*n*-butyl acrylate/heptadecafluorodecyl methacrylate (*p*-MMA/nBA/FMA), and *p*-methyl methacrylate/*n*-butyl acrylate/heptadeca fluorodecyl acrylate (*p*-MMA/nBA/FA). These studies consist of two parts: (1) colloidal particle synthesis and molecular modeling and (2) coalescence of F-containing particles.

Experimental Section

MMA, nBA, FBMA, FBA, FMA, FA, potassium persulfate (KPS), and sodium dodecyl sulfate (SDS) were purchased from

*Author to whom all correspondence should be addressed. E-mail: marek.urban@usm.edu.

 Published on Web 10/02/2009

Table 1. Composition, Molecular Weight, and Particle Size Analysis of Colloidal Dispersions Containing *p*-MMA/nBA (A), *p*-MMA/nBA/FBMA (B), *p*-MMA/nBA/FBA (C), *p*-MMA/nBA/FMA (D), and *p*-MMA/nBA/FA (E) Copolymers[a]

	p-MMA/nBA A	*p*-MMA/nBA/FBMA B	*p*-MMA/nBA/FBA C	*p*-MA/nBA/FMA D	*p*-MMA/nBA/FA E
MMA (w/w %)	19.5	16.5	16.5	16.5	16.5
nBA (w/w %)	19.5	16.5	16.5	16.5	16.5
F-monomer (w/w %)	0	5.9	5.9	5.9	5.9
SDS (w/w %)	1.5	1.5	1.5	1.5	1.5
DLPC (w/w %)	0.26	0.26	0.26	0.26	0.26
DDI (w/w %)	59.2	59.2	59.2	59.2	59.2
KPS (w/w %)	0.23	0.23	0.23	0.23	0.23
mol wt (g/mol) $\times 10^{-5}$	0.96	0.93	0.95	1.05	1.15
solids content (w/w %)	41	41	41	41	41
F-polymer content (w/w %)	0	15	15	15	15
particle size (nm)	100	110	102	130	128

[a] The amount of the fluoropolymer phase in *p*-MMA/nBA/FBMA (B), *p*-MMA/nBA/FBA (C), *p*-MMA/nBA/FMA (D), and *p*-MMA/nBA/FA (E) is 15% w/w which was confirmed by solid content analysis and cross-polarization ^{19}F and ^{13}C with ^{1}H and ^{19}F decoupling solid state NMR experiments (details are provided in the Supporting Information). The solid content measurements after polymerization confirmed that 15% fluoromomers initially added during synthesis have been completely polymerized.

Aldrich Chemical Co. 1,2-Dilauroyl-*sn*-glycero-3-phosphocholine (DLPC) phospholipid was purchased from Avanti Polar Lipids, Inc. *p*-MMA/nBA/FBMA, *p*-MMA/nBA/FBA, *p*-MMA/nBA/FMA, and *p*-MMA/nBA/FA emulsions were synthesized using a semicontinuous process outlined elsewehere,[19,22] and adapted for a small-scale polymerization. The reaction flask was placed in a water bath set at 78 °C, purged with N_2 gas, and charged with 20 mL of DDI water under continuous stirring at 300 rpm. SDS and DLPC surfactants were utilized, and Table 1 provides the ratio of all dispersions prepared for the purposes of these studies. Surfactants were dissolved in water under high agitation followed by addition of monomers to produce a semistable pre-emulsion. For seeded emulsion process, 10% (w/w) of the pre-emulsion and 18% (w/w) of the initiator solution were initially injected into the reaction kettle, thus facilitating the seed formation. The remaining pre-emulsion was fed continuously over the period of 4 h while the initiator solution was added for 4.5 h. Upon completion of the initiator feed, polymerization was allowed to continue for another 5 h. This process resulted in 40.5% w/w solids which was determined from the initial feed composition of the initiator monomer mixture and the analysis of the solid content after the synthesis.

The particle size analysis was obtained using a Microtrac UPA 250 instrument. Morphologies of colloidal particles were determined using a Zeiss EM 109-transmission electron microscope (TEM) in which colloidal dispersions were diluted to a 10,000:1 vol. ratio (DDI H_2O: dispersions) and deposited on a Formvar coated copper TEM grid (Ted Pella, Inc.). Table 1 illustrates composition, molecular weight, solid content, and particle sizes of colloidal dispersions of *p*-MMA/nBA/FBMA, *p*-MMA/nBA/FBA, *p*-MMA/nBA/FMA, and *p*-MMA/nBA/FA.

Colloidal particle solutions were allowed to coalesce for 72 h in a controlled environment at 23 °C temperature and 60% relative humidity (RH) to form approximately 10 μm thick films. The films were obtained by draw down on the polyvinyl chloride substrates. For contact angle measurements colloidal solutions were coalesced on glass slide using a draw bar to give an approximately film thickness of 10 μm. Molecular weight was determined using gel permeation chromatography (GPC) system which consists of a Waters Alliance 2695 separation module, a Waters 2410 interferometric refractometer, and two PL HFIPgel (Polymer Laboratories Inc.) GPC columns connected in series. Freshly distilled HFIP serves as the mobile phase with a flow rate of 1.0 mL/min. Sample concentrations were 10−12 mg/mL in freshly distilled HFIP, with an injection volume of 50 μL. The detector signals were recorded using Empower 2 Chromatography Data Software (Waters Corporation), and molecular weights were determined relative to narrow molecular weight *p*-MMA standards.

Solid-state ^{19}F NMR measurements were performed on a Varian ^{UNIT}YINOVA 400 spectrometer using a standard Chemagnetics 7.5 mm PENCIL-style probe. Samples were loaded into zirconia rotor sleeves, sealed with Teflon caps, and spun at a rate of 4.5 kHz. The standard cross-polarization magic angle spinning (CP/MAS) technique was used with high-power proton decoupling implemented during data acquisition. The acquisition parameters were as follows: The ^{1}H 90° pulse width was 4.0 μs, the cross-polarization contact time was 3.5 ms, the dead time delay was 6.4 μs, and the acquisition time was 45 ms.[23] A recycle delay of 3 s between scans was utilized. Experiments requiring simultaneous ^{1}H and ^{19}F decoupling were performed using a 3.2 mm HFXY probe. The ^{1}H and ^{19}F 90° pulse widths were 4.0 ms, the acquisition time was 26 ms, and the $^{19}F-^{13}C$ cross-polarization contact time was 10 ms. A recycle delay of 2 s and a samples spinning rate of 5 kHz were used.

Internal reflection infrared imaging (IRIRI) experiments were conducted on a Varian Stingray system. This system consists of a Bio-Rad FTS 6000 spectrometer, a UMA 500 microscope, an Image IR focal plane array (FPA) image detector, and a semispherical germanium IRE. IRIR images were collected using the following spectral acquisition parameters: under sampling ratio 2, step-scan speed 5 Hz, and spectral resolution 8 cm^{-1}, and the use of a Ge crystal in contact with the analyzed surface allows spatial resolution in the range of 1 μm.[24] In a typical experiment, spectral data set acquisition time was 2 min and image processing was performed using ENVI software (The Environment for Visualizing Images, Research Systems, Inc.) version 3.5. When appropriate, baseline correction algorithms were applied to compensate for baseline deviations which were accomplished by built-in application software supplied by GRAMS/A1 v 7.02 (Galactic Ind.). Contact angle measurements were obtained using a FTA200 dynamic contact angle analyzer using water as solvent, and a Qualitest 1055 friction tester was utilized to determine the coefficients of friction.[25]

Quantum mechanical semiempirical calculations were conducted using Material Studio software (Accerlrys Inc., version 4.1). Computer modeling simulations were performed using a classical (Newton) molecular dynamics theory combined with the COMPASS force field conditions. In the first step, we created an alternate polymeric unit of MMA and nBA consisting of four monomer units of each, followed by block copolymerization of fluoropolymer (two monomer units). In an effort to determine thermodynamic response of molecular segments, a 25 × 25 × 25 Å periodic unit cell was constructed at 298 K using eight polymeric chains of block copolymerized fluoropolymers with *p*-MMA/nBA units. After amorphous cell construction first the control parameter were number, volume, and temperature (*NVT*) (298 K, 25 ps dynamic time, 25000 number of steps, and frame output at every 1000 steps), and second step was to control number, pressure, temperature (NPT) (298 K, 50 ps dynamic time, 50000 number of steps, and frame output at every 5000 steps) to determine the change in volume and total energy required for the cell construction with varying chain length of

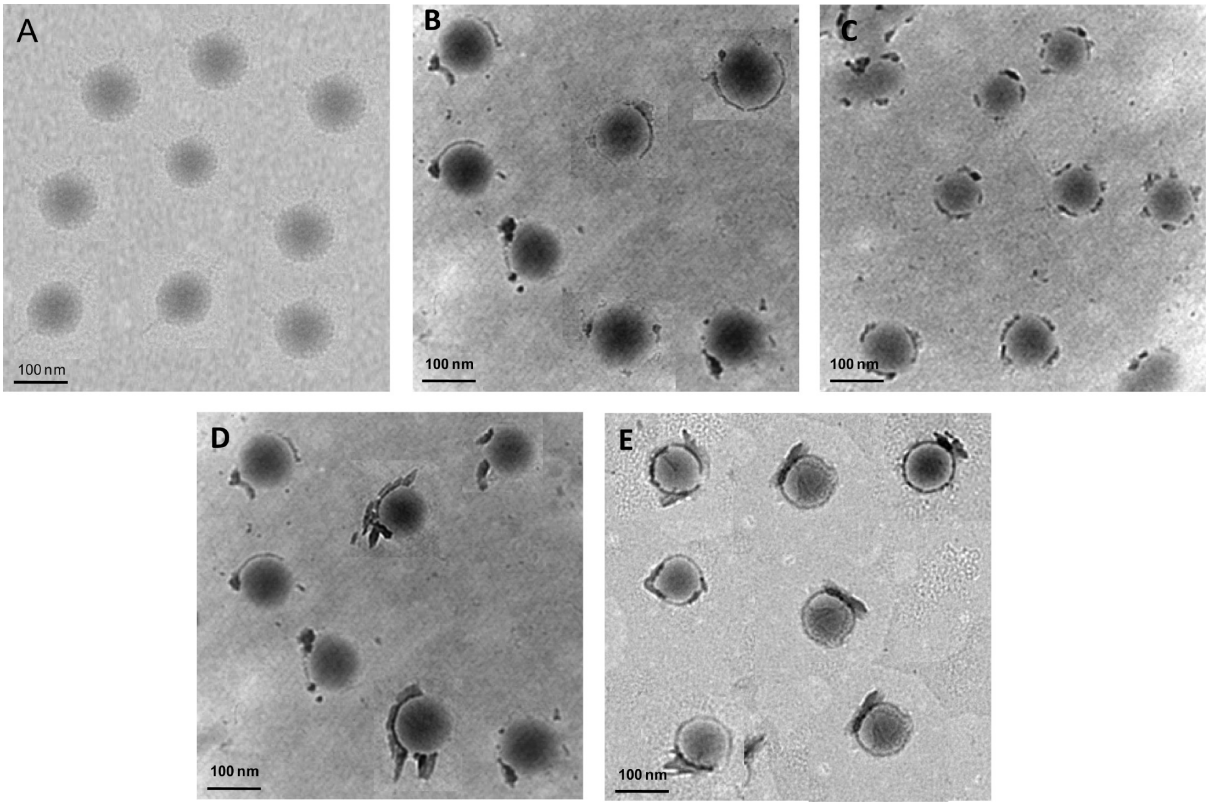

Figure 1. Transmission electron micrographs of colloidal particles containing (A) *p*-MMA/nBA, (B) *p*-MMA/nBA/FBMA, (C) *p*-MMA/nBA/FBA, (D) *p*-MMA/nBA/FMA, and (E) *p*-MMA/nBA/FA copolymers.

perfluoroalkyl side chain of fluoromonomers. Cohesive energy density (CED) was determined by using forcite calculations after the NPT cell construction was performed. Binding energies of surfactants and polymer associations were calculated by taking binding energy of the fluoropolymer associated with the surfactant and subtracting it from the binding energy of the polymer and the surfactant.

Results and Discussion

Colloidal Particle Synthesis and Modeling. As stated in the Introduction, the main objective of these studies was to synthesize *p*-MMA/nBA/FBMA, *p*-MMA/nBA/FBA, *p*-MMA/nBA/FMA, and *p*-MMA/nBA/FA colloidal particles without the use of F-containing dispersing agents. Such prepared dispersions were synthesized using traditional free radical emulsion polymerization process, and as listed in Table 1, the particle size ranges from 102 to 130 nm. As the perfluoroalkyl side chain length of monomers increases, the particle size also increases. Figure 1 illustrates TEM images of individual particle morphologies of *p*-MMA/nBA (A), *p*-MMA/nBA/FBMA (B), *p*-MMA/nBA/FBA (C), *p*-MMA/nBA/FMA (D), and *p*-MMA/nBA/FA (E) particles and, as seen in Image A, *p*-MMA/nBA particles exhibit spherical shape. However, upon copolymerizing FBMA, FBA, FMA, and FA with MMA/nBA monomers, the particle morphology changes. The observed high electron density regions observed in images B−E of Figure 1 show the exterior of the *p*-MMA/nBA core being the FP phase, thus forming intraparticle phase-separated nonspherical shapes. These data also show that by increasing the length of the perfluoroalkyl side chain from $(CF_2)_2CF_3$ to $(CF_2)_7CF_3$, when going from FBMA to FMA monomers, not only the size of the particles increases, but the phase-separated FP domains within each particle also increase. The results of these studies are in agreement with the previous findings, in which F-surfactants were utilized in the synthesis of fluorine-containing colloidal dispersions,[18−20] and also resulted in the phase separated heterogeneous nonspherical colloidal particles.

Although the origin of the phase separation and nonspherical morphologies of colloidal particles containing FP prepared in the presence of fluorosurfactants have been proposed,[17−19] we are also interested in determining the location of the FP phase on the *p*-MMA/nBA particle core. Solid state NMR results shown in Figure S-1 of the Supporting Information confirm block copolymerization of the FP phase on the *p*-MMA/nBA/FP copolymer particle surfaces. While TEM and NMR measurements established phase separation regions and the copolymer type, formation of FP phase domains within one particle needs further consideration. Conceptually, one can envision that when polymerization is carried out under monomer starvation conditions, it is expected that the monomer hydrophobicity and solubility differences facilitates F-monomer migration to the reactive site at the later stages of the polymerization, thus leading to block copolymerization of the FP phase.[17] Also, the presence of SDS and DLPC dispersing agents on the surface of the *p*-MMA/nBA core provides another possibility for F-monomer polymerization on the surface areas of the *p*-MMA/nBA core with an access of DLPC creating energetically favorable conditions for copolymerization.

To support experimental data we utilized computer modeling in which molecular thermodynamics simulations were employed for *p*-MMA/nBA, *p*-MMA/nBA/FBMA, *p*-MMA/nBA/FBA, *p*-MMA/nBA/FMA, and *p*-MMA/nBA/FA copolymer to determine energetic requirements for each copolymer. The unit cells were constructed using packing energy minimized polymer chains under 3D periodic boundary conditions and the details of the computational analysis are provided in the Experimental Section. The visual

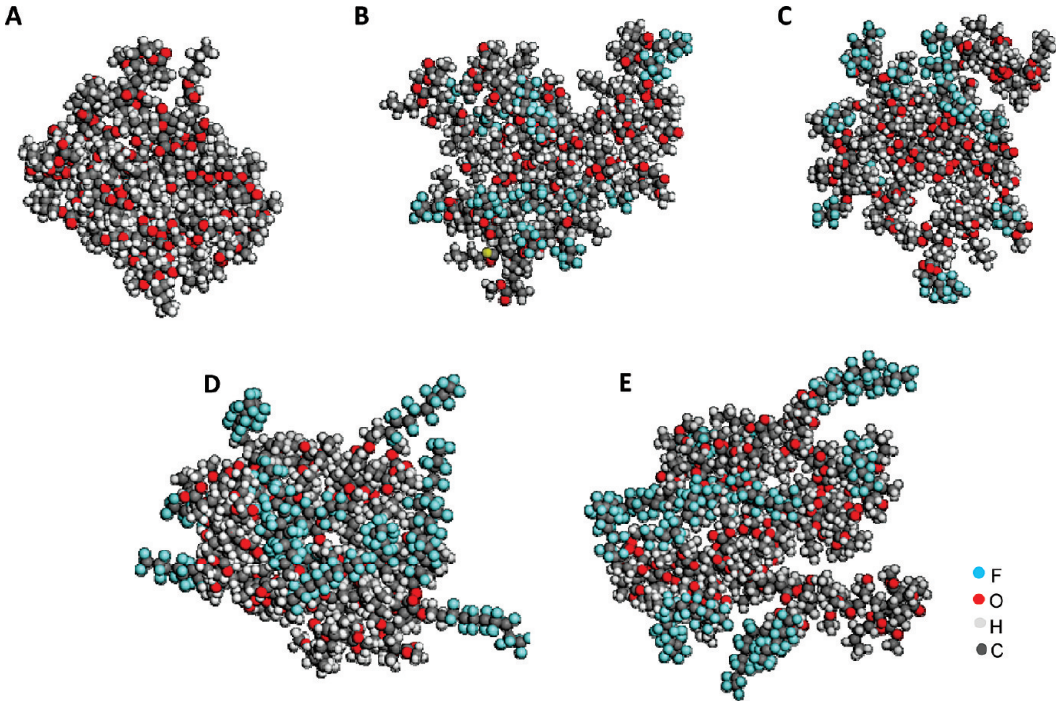

Figure 2. Results of computational simulations leading to significant volume and conformational changes for (A) *p*-MMA/nBA, (B) *p*-MMA/nBA/FBMA, (C) *p*-MMA/nBA/FBA, (D) *p*-MMA/nBA/FMA, and (E) *p*-MMA/nBA/FA copolymers.

Table 2. Volume, Energy, and Cohesive Energy Density Calculations for *p*-MMA/nBA, *p*-MMA/nBA/FBMA, *p*-MMA/nBA/FBA, *p*-MMA/nBA/FMA, and *p*-MMA/nBA/FA Copolymers

copolymer composition	volume (nm^3)	total energy (kcal/mol)	potential energy (kcal/mol)	kinetic energy (kcal/mol)	cohesive energy density (J/cm^3)
p-MMA/nBA	12.9	3779	2652	1127	254
p-MMA/nBA/FBMA	15.1	3651	2453	1198	221
p-MMA/nBA/FBA	14.8	3356	2193	1163	218
p-MMA/nBA/FMA	19.0	3004	1582	1422	203
p-MMA/nBA/FA	18.7	2675	1295	1380	192

representation of the results of the analysis is depicted in Figure 2, parts A−E, for *p*-MMA/nBA (A), *p*-MMA/nBA/FBMA (B), *p*-MMA/nBA/FBA (C), *p*-MMA/nBA/FMA (D), and *p*-MMA/nBA/FA (E), respectively. As seen, by incorporating F-monomers, significant conformational changes are observed within the amorphous cell. Comparison of *p*-MM/nBA (A) with *p*-MM/nBA/FBMA (B) and *p*-MM/nBA/FBA (C) morphologies shows that the FP phase is less compact, exhibit larger particle size, and is spatially extended due to larger to larger perfluoroalkyl side chain length, as shown for *p*-MM/nBA/FMA (D) and *p*-MM/nBA/FA (E). Also, a greater degree of surface phase separation is observed. These predictions are in agreement with the experimentally observed TEM images shown in Figure 1 and the measurements of the particle size listed in Table 1. The total volume changes increase from 12.9 nm^3 for *p*-MMA/nBA to 15.1 and 14.8 nm^3 for *p*-MMA/nBA/FBMA and *p*-MMA/nBA/FBA, respectively, and 19.0 nm^3 for *p*-MMA/nBA/FMA, which is related to the perfluoroalkyl side chain lengths of fluoromonomers (FBA being the shortest and FMA being the longest).

The total energies (G) required to obtain copolymer packing of the individual unit cells are listed in Table 2. For *p*-MMA/nBA copolymer, the G values comprised of the potential energy (E_{pot}) and the kinetic energy (E_{kin}) is 3779 kcal/mol. Upon incorporating the *p*-FBMA phase, the G value decreases by 128 kcal/mol (from 3779 to 3651 kcal/mol). At the same time, the E_{pot} decreases by 199 kcal/mol, but the E_{kin} is elevated by 71 kcal/mol. These results show that the incorporation of the FP phase results in thermodynamically, but not kinetically favorable compositions. Since the E_{pot} changes account for conformational polymer changes, energetically favorable conformations for the FP occur when the FP segments are on the exterior of the *p*-MMA/nBA particle surface. In contrast, the E_{kin} changes account for the ease of altering conformational arrangements. As the FP phase content increases due to FMA and FA copolymerization, the total energy is reduced due to the reduction of the potential energy to attain most stable conformations illustrated in Figure 2. Also, the decrease of the G values upon incorporation of the FP phase is attributed to their lower surface energy, hence the incorporation of the FP phase into copolymer structure leads to the reduction of the total energy, as the system approaches more stable phase-separated configuration.

In order to estimate whether block or random copolymerization of MMA, nBA, and fluoromonomers are favorable, similar modeling experiments were conducted on block and random copolymers of *p*-MMA/nBA/FP. The amorphous cell construction incorporated formation of random *p*-MMA/nBA/FP copolymers, followed by *NVT* and *NPT* thermodynamic calculations. Although these calculations showed that for random copolymer structures the G values change by only ±25 kcal/mol from a blocked copolymer, these calculations do not take into account the presence of dispersing agents which, as will be seen later, will play a significant role in the two-phase systems.

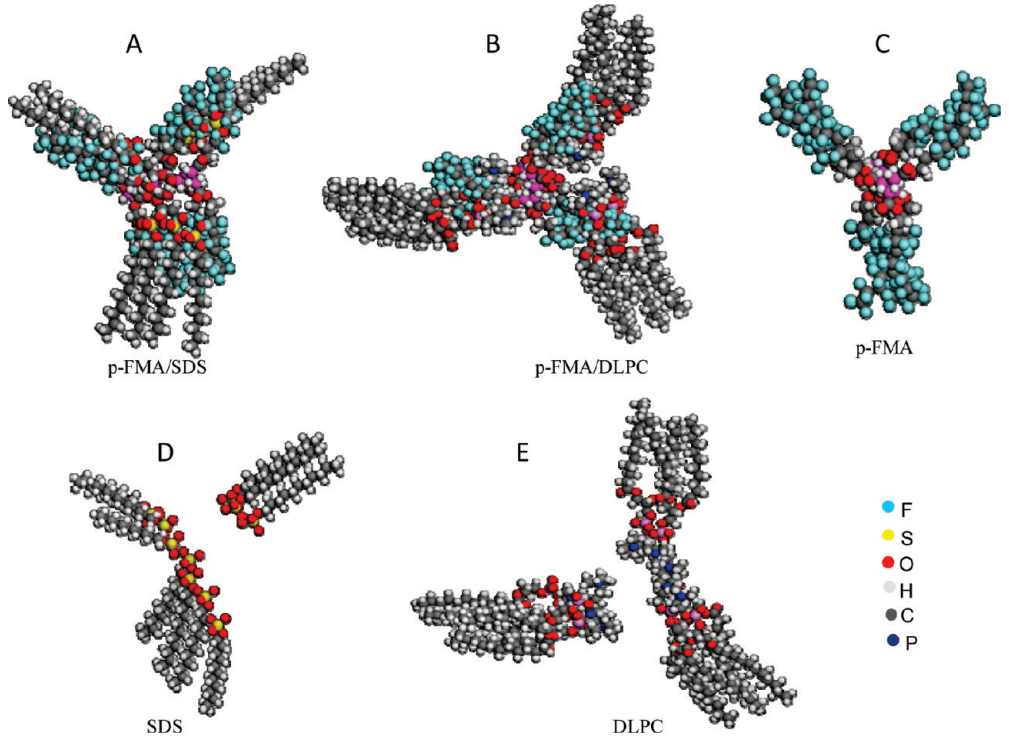

Figure 3. Molecular structures of (A) *p*-FMA associations with SDS, (B) *p*-FMA associations with DLPC, (C) *p*-FMA, (D) SDS, and (E) DLPC To obtain association energy values for *p*-FMA/SDS and *p*-FMA/DLPC, calculated energies of *p*-FMA, SDS, and DLPC were subtracted from the total energies of *p*-FMA/SDS and *p*-FMA/DLPC.

Table 3. Binding Energy Calculations for *p*-MMA/nBA, *p*-FBMA, *p*-FBA, *p*-FMA, and *p*-FA Copolymers with SDS and DLPC Association

composition	*p*-MMA/nBA	*p*-FBMA	*p*-FBMA	*p*-FMA	*p*-FA
binding energy with SDS (kcal/mol)	−408	−247	−219	−366	−317
binding energy with DLPC (kcal/mol)	−907	−1657	−1472	−2441	−2154

To determine the amount of energy is required to remove one polymer chain from *p*-MMA/nBA, *p*-MMA/nBA/FBMA, *p*-MMA/nBA/FBA, *p*-MMA/nBA/FMA, and *p*-MMA/nBA/FA copolymer cells, we calculated the cohesive energy density (CED) which represents the amount of energy required to completely isolate a polymer chain as a function of composition. As shown in Table 2, the CED changes determined for different copolymer compositions show that the smaller values are obtained for the FP containing copolymers. In contrast, the CED values for *p*-MMA/nBA copolymer are the largest, compared to the copolymers containing the FP phase. This is attributed to the fact that the FP is phase-separated and less energy is required to separate individual polymeric chains. Furthermore, the decrease of the CED is proportional to the amount of the F-content in the backbone of the copolymer structure, reaching the value of 192 J/cm^3 for *p*-MMA/nBA/FA.

Because of useful properties of FPs it is desirable to incorporate as much of the FP phase as possible. However, for *p*-MMA/nBA/FP colloidal particles the limiting factor is the stability of colloidal dispersions. As indicated in the Experimental Section, we utilized bioactive PLs which form mixed micellar entities with SDS without the use of F-containing dispersing agents. PLs, being main constituents of the cell membranes, serve as selective barriers for bioactive species as well as providing support for membrane protein transport.[26] As was shown in the literature, PLs along an SDS form miscible micellar structures, the FP phase growth on the *p*-MMA/nBA colloidal particles is facilitated by the reduction of the overall surface tension of the aqueous phase from 72 to about 1−5 mN/m.[27,28] This was the primary reason for choosing DLPC as one of the dispersing agents during colloidal synthesis, thus allowing *p*-MMA/nBA seed formation, followed by employing the monomer starvation conditions, forced F-monomers to migrate to reactive sites. Since PLs exhibit dual functions: they facilitate transport of F-monomers to the *p*-MMA/nBA core and stabilize the growing particles, thus eliminating the use of F-surfactants.

It is also important to determine the location of SDS and DLPC on the surface of colloidal particles. If the presence of DLPC facilitates the growth of the FP phase on the surface of *p*-MMA/nBA, DLPC should exhibit energetically favorable interactions with the FP phase. Since SDS and DLPC form miscible micellar structures,[20] we determined the binding energy for the association of SDS and DLPC molecules with *p*-MMA/nBA and FP segments using computer modeling simulations. Figure 3 shows the results of the modeling experiments in which the total energies of *p*-FMA/SDS and *p*-FMA/DLPC were calculated (Figure 3, A and B). The same calculations were independently conducted for *p*-FMA (C), SDS (D), and DLPC (E), while maintaining conformations of *p*-FMA/SDS and *p*-FMA/DLPC. These values were subtracted from the total energies of *p*-FMA/SDS and *p*-FMA/DLPC, respectively. To obtain energies responsible for *p*-FP/SDS and *p*-MMA/nBA interactions, similar calculations were conducted for *p*-MMA/nBA, *p*-FBMA, *p*-FBA, and *p*-FA. The results are summarized in Table 3. As seen, favorable associations (higher negative values) are observed between the polymer and the dispersing agent molecules. Specifically, these associations are more

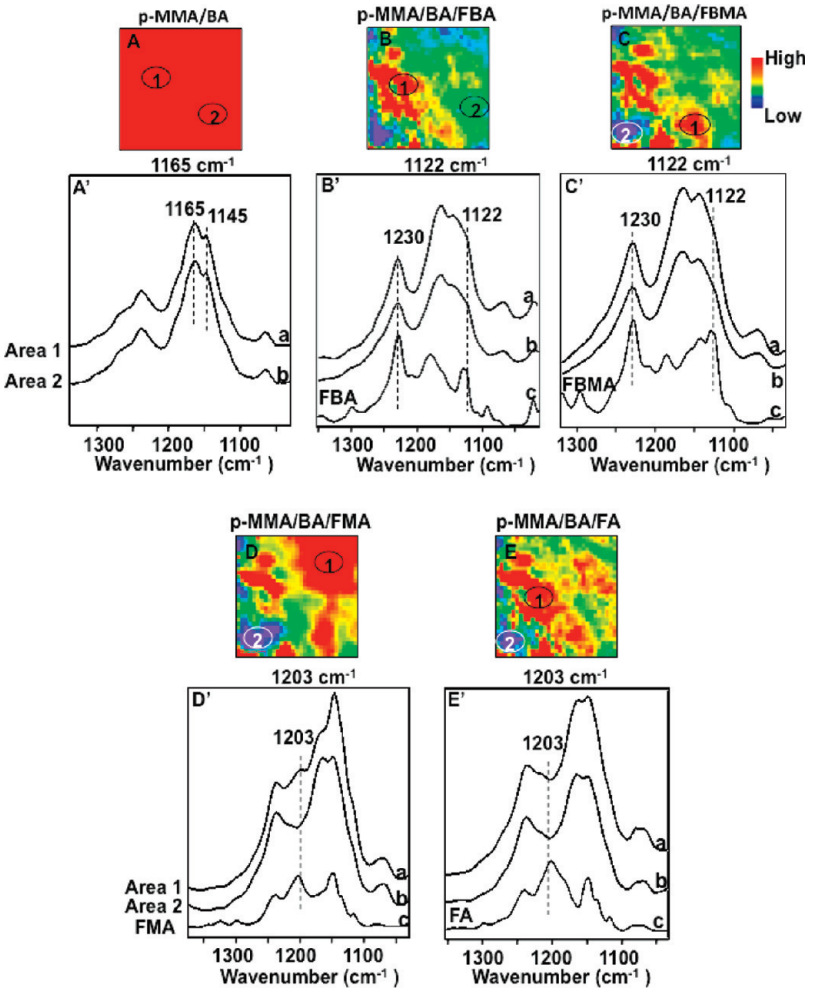

Figure 4. IRIR images recorded from the F−A interface of films obtained from (A) *p*-MMA/nBA colloidal dispersions (A, IR image obtained by tuning into the 1165 cm^{-1} band; A′, traces a and b, IR spectra recorded from areas labeled 1 and 2 in image A, respectively); (B) *p*-MMA/nBA/FBA colloidal dispersions (B, IR image obtained by tuning into the 1122 cm^{-1} band; A′, traces a and b, IR spectra recorded from areas labeled 1 and 2 in image B; trace c representing the IR spectrum of FBA); (C) *p*-MMA/nBA/FBMA colloidal dispersions; (C, IR image obtained by tuning into the 1122 cm^{-1} band; C′, traces a and b, IR spectra recorded from areas labeled 1 and 2 in image C; Trace c represents the IR spectrum of FBMA; (D) *p*-MMA/BA/FMA colloidal dispersions; (D, IR image obtained by tuning into the 1203 cm^{-1} band; D′, traces and b, IR spectra recorded from areas labeled 1 and 2; Trace c represents IR spectrum of FMA); (E) *p*-MMA/BA/FA colloidal dispersions; (E, IR image obtained by tuning into the 1203 cm^{-1} band; E′, Ttraces and b, IR spectra recorded from areas labeled 1 and 2; trace c representing the IR spectrum of FA).

favorable for *p*-MMA/nBA than for the FP-SDS interactions. The FP-DLPC pair also exhibits favorable interactions compared to *p*-MMA/nBA, giving raise to more negative binding energies for the long chain perfluoroalkyl side chain FPs. Thus, based on the binding energy calculations for the mixed micellar structures, PL molecules exhibit energetically more favorable associations with the FP phase, whereas SDS prefer binding with the *p*-MMA/nBA phase.

Coalescence of *p*-MMA/nBA/PF Particles. As shown in the previous studies,[18−20] particle morphologies and dispersing agents play a significant role in particles coalescence. In an effort to identify surface chemical composition of films prepared from *p*-MMA/nBA/FP and to determine distribution of the FP phase at the F−A interface, we utilized IRIR imaging. The results of these experiments are shown in Figure 4, images A−F. Figure 4A illustrates the IR image of the F−A interface of *p*-MMA/nBA, which was generated by tuning into the 1165 cm^{-1} band due to C−O−C stretching vibrations of *p*-nBA at 1 μm level spatial resolution, no compositional variations are detected and highly uniform films with no phase separation are produced, as confirmed in Figure 4A′ by the analysis of the IR spectrum recorded from areas 1 and 2 with no changes of the 1165 and 1145 cm^{-1} bands due to nBA and MMA components, respectively. Figure 4B illustrates the IR image of the F−A interface of *p*-MMA/nBA/FBMA, which was generated by tuning into the 1122 cm^{-1} band due to C−F stretching vibrations. As seen, the C−F stretching bands of the copolymer matrix are detected and their distribution is heterogeneous, with the regions consisting of the higher concentration levels of the C−F moieties. While the IR image in Figure 4B provides spatial distributions of the chemical entities near the F−A interface, Figure 4B′ represents averaged IR spectra obtained from the areas labeled 1 and 2 in Figure 4B. As seen, area 1 is largely saturated by the C−F groups, as manifested by the higher intensities of the 1122 and 1230 cm^{-1} bands, thus signifying the presence of the FP phase. However, the same band exhibits lower intensity in area 2, as shown in trace b. For reference purposes, trace c is the spectrum of FBMA.

The same analysis was conducted on *p*-MMA/nBA/FBA, *p*-MMA/nBA/FMA, and *p*-MMA/nBA/FA films, and the results of these experiments are displayed in Figure 4, C-E, respectively. Chemical mapping using IRIRI of these surfaces (Images C-E) shows again heterogeneous morphologies, where the FP phase (red color) forms islands at the

Table 4. Advancing, Static, and Receeding Contact Angles for *p*-MMA/nBA, *p*-MMA/nBA/FBMA, *p*-MMA/nBA/FBA, *p*-MMA/nBA/FMA, and *p*-MMA/nBA/FA Films Obtained from Coalesced Colloidal Particles

composition	advancing contact angle (deg)	static contact angle (deg)	receeding contact angle (deg)
p-MMA/BA	75	65	50
p-MMA/BA/ FBMA(15%)	102	99	87
p-MMA/BA/ FBA(15%)	100	94	85
p-MMA/B A/ FMA(15%)	112	104	98
p-MMA/BA/ FA(15%)	110	102	97

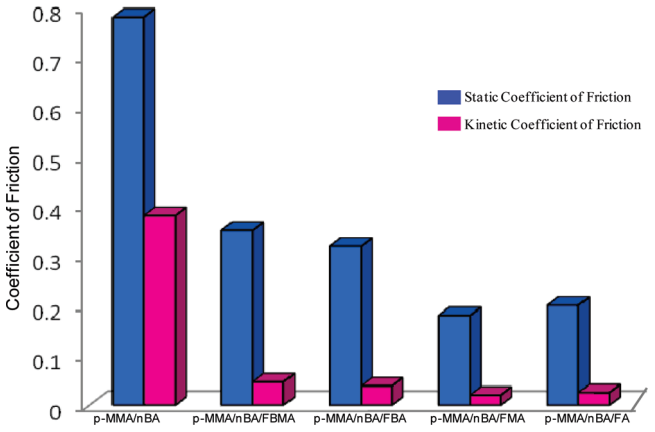

Figure 5. Static and kinetic coefficients of friction for *p*-MMA/nBA, *p*-MMA/nBA/FBMA, *p*-MMA/nBA/FBA, *p*-MMA/nBA/FMA, and *p*-MMA/nBA/FA films plotted for each copolymer colloidal composition.

F−A interface. IR analysis of areas 1 and 2 also shows that area 1 consists of the higher concentration levels of the FP phase, as manifested by the IR spectra shown in traces a and b. Traces c in Figure 4, B′-E′ represent IR spectra of respective F-monomers. These results again illustrate the development of heterogeneous phase-separated surfaces for FP containing films, in which FP phase migrates to the F−A interface during film formation.

To elucidate how stratification affects film interfacial properties, contact angle and coefficient of friction measurements were conducted. Table 4 provides advancing, static, and receeding contact angle results for *p*-MMA/nBA, *p*-MMA/nBA/FBMA, *p*-MMA/nBA/FBA, *p*-MMA/nBA/FMA, and *p*-MMA/nBA/FA copolymer compositions. For *p*-MMA/nBA films, the static water contact angle is 65°, which upon incorporation of the FP phase increases to 98° for *p*-MMA/nBA/FBMA, 94° for *p*-MMA/nBA/FBA, 105° for *p*-MMA/nBA/FMA, and 104° for *p*-MMA/nBA/FA films. This increase appears to be directly related to the perfluoroalkyl side chain length of the fluoromonomers utilized in the synthesis. As anticipated, static and kinetic coefficients of friction also change significantly. As shown in Figure 5, the static coefficient of friction is reduced from 0.78 for *p*-MMA/nBA to 0.18 for *p*-MMA/nBA/FMA films. Also, the kinetic coefficient of friction is reduced from 0.38 to 0.02, thus exceeding polytetrafluoroethylene (0.04).[29] The static coefficient of friction is relatively high due to the presence of *p*-MMA/nBA component which provides significant adhesiveness during the static measurements, but longer perfluoroalkyl chains result in the lowest static and kinetic coefficients of frictions.

We also analyzed surface components using ATR-FTIR spectroscopy and specifically examined mobility and stratification of dispersing agents near the F−A interface. Figure S-2 in the Supporting Information shows a series of polarized ATR-FTIR spectra recorded from the F−A interface of *p*-MMA/nBA/FBMA (A), *p*-MMA/nBA/FBA (B), *p*-MMA/nBA/FMA (C), and *p*-MMA/nBA/FA (D), and preferentially perpendicular orientation with respect to the F−A interface is shown for SDS and DLPC.[30−33] These observations agree with the computational binding energy predictions tabulated in Table 3. Since the FP phase at the surface of colloidal particles is stabilized by DLPC and SDS, during coalescence, as the FP phase stratifies near the F−A interface during coalescence, SDS and DLPC associated with the FP phase also migrate to this interface. As shown by the computer modeling experiments, longer perfluoroalkyl side chains exhibit favorable interactions between the FP phase and DLPC, as demonstrated by the lower (FP/DLPC) binding energies listed in Table 3.

Conclusions

The utilization of SDS/DLPC dispersing agents facilitates green synthesis of acrylics and methacrylics F-monomers using classical emulsion polymerization process without the use of F-surfactants. Computer simulations and experimental results show that the FP phase forms energetically favorable phase-separate entity on the surface of *p*-MMA/nBA. The presence of the FP phase results in the decrease of the cohesive energy density of macromolecular chains. Polymeric films obtained as a result of the coalescence of *p*-MMA/nBA/FP self-stratify, with the FP phase being near the F−A interface to form phase-separated domains of fluorinated and nonfluorinated layers resulting in low coefficients of frictions.

Acknowledgment. Major support for these studies from the National Science Foundation Materials Research Science Engineering Center (NSF MRSEC) (DMR 0213883) is acknowledged. The authors also acknowledge use of instrumentation and facilities through the Materials Research Facilities Network (MRFN) supported by the NSF MRSEC program (DMR 0213883) as well as Major Research Instrumentation program DMR 0215873.

Supporting Information Available: Figures showing and text dicussing solid state ^{19}F and ^{13}C NMR cross-polarized spectra with ^{1}H and ^{19}F decoupling of *p*-MMA/nBA/FBMA copolymer as well as polarized attenuated total reflectance (ATR) FT-IR spectra recorded from the film−air interfaces of *p*-MMA/nBA, *p*-MMA/nBA/FBMA, *p*-MMA/nBA/FBA, *p*-MMA/nBA/FMA, and *p*-MMA/nBA/FA copolymers are available free of charge via Internet at http://pubs.acs.org.

References and Notes

(1) Solomon, S.; Garcia, R. R.; Sherwood, F.; Wuebbles, D. J. *Nature* **1986**, *321*, 755.
(2) DeSimone, J. M.; Guan, Z.; Elsbernd, C. S. *Science* **1992**, *257*, 945.
(3) DeSimone, J. M.; Maury, E. E.; Menceloglu, Y. Z.; McClain, J. B.; Romack, T. J.; Combes, J. R. *Science* **1994**, *265*, 356.
(4) McClain, J. B.; Betts, D. E.; Canelas, D. A.; Samulski, E. T.; DeSimone, J. M.; Londono, J. D.; Cochran, H. D.; Wignall, G. D.; Chillura-Martino, D.; Triolo, R. *Science* **1996**, *274* (5295), 2049–2051.
(5) Romack, T. J.; DeSimone, J. M.; Treat, T. A. *Macromolecules* **1995**, *28*, 8429.
(6) Michel, U.; Resnick, P.; Kipp, B.; DeSimone, J. M. *Macromolecules* **2003**, *36*, 7107.
(7) Hyatt, J. A. *J. Org. Chem.* **1984**, *49*, 5097.
(8) Koendrick, G. H.; Sacanna, S.; Pathmamanoharan, C.; Rasa, M.; Philipse, A. P. *Langmuir* **2001**, *17*, 6086.

(9) Ha, J.; Park, I.; Lee, S.; Kim, D. *Macromolecules* **2002**, *35*, 6811.
(10) Thomas, R. R.; Lloyd, K. G.; Stika, L. M.; Stephens, L. E.; Megallanes, G. S.; Dimonie, V. L.; Sudol, E. D.; El-Aasser, M. S. *Macromolecules* **2000**, *33*, 8828.
(11) Landfester, K.; Rothe, R.; Antonietti, M. *Macromolecules* **2002**, *35*, 1658.
(12) Cinar, H.; Kretschmann, O.; Ritter, H. *Macromolecules* **2005**, *38*, 5078.
(13) Lau, W. *Macromol. Symp*. **2002**, *182*, 283.
(14) Wood, C. D.; Senoo, K.; Martin, C.; Cuellar, J.; Cooper, A. I. *Macromolecules* **2002**, *35*, 6743.
(15) Linemann, R. F.; Malner, T. E.; Brandsch, R.; Bar, G.; Ritter, W.; Mulhaupt, R. *Macromolecules* **1999**, *32*, 1715.
(16) Sacanna, S.; Koenderink, G. H.; Philipse, A. P. *Langmuir* **2004**, *20*, 8398.
(17) Misra, A.; Jarrett, W. L.; Urban, M. W. *Macromolecules* **2007**, *40*, 6190.
(18) Dreher, W. R.; Singh, A.; Urban, M. W. *Macromolecules* **2005**, *38*, 4666.
(19) Dreher, W. R.; Jarrett, W. L.; Urban, M. W. *Macromolecules* **2005**, *38*, 2205.
(20) Singh, A.; Dreher, W. R.; Urban, M. W. *Langmuir* **2006**, *22*, 524.
(21) Dreher, W. R.; Urban, M. W. *Langmuir* **2004**, *20*, 10455.
(22) Davis, S. D.; Hadgraft, J.; Palin, K. J. *Encyclopedia of Emulsion Technology*. Marcel Dekker: New York, 1985; Vol. *2*.
(23) Schaefer, J.; Stejskal, E. O.; Buchdahl, R. *Macromolecules* **1977**, *10*, 384.
(24) Otts, D.; Zhang, P.; Urban, M. W. *Langmuir* **2002**, *18*, 6473.
(25) Evanson, K. W.; Thortenson, T. A.; Urban, M. W. *J. Appl. Polym. Sci*. **1991**, *42*, 2309.
(26) Voet, D.; Voet, J. G. *Biochemistry*. 1st ed.; Wiley & Sons, Inc.: New York, 1995.
(27) Nii, T.; Ishii, F. *Colloids Surf*. **2004**, *39*, 57.
(28) Pinazo, A.; Wen, X.; Liao, Y. C.; Prosser, A. J.; Franses, E. I. *Langmuir* **2002**, *18*, 8888.
(29) Brandrup, J.; Immergut, E. H. *Polymer Handbook*. 2nd ed.; John Wiley & Sons: New York, 1966.
(30) Silverstein, R. M.; Webster, F. X. *Spectrometeric Indentification of Organic Compounds*. John Wiley and Sons: New York, 1998.
(31) Lestage, D. J.; Urban, M. W. *Langmuir* **2005**, *21*, 2150.
(32) Lestage, D. J.; Yu, M.; Urban, M. W. *Biomacromolecules* **2005**, *6*, 1561.
(33) Dreher, W. R.; Urban, M. W. *Langmuir* **2003**, *19*, 10254.